JEE Journal of Ecological Engineering

Journal of Ecological Engineering 2023, 24(6), 54–64
https://doi.org/10.12911/22998993/162400
ISSN 2299–8993, License CC-BY 4.0

Received: 2023.03.03
Accepted: 2023.04.17
Published: 2023.05.01

# Estimation of Suspended Sediment Load Using Artificial Neural Network in Khour Al Zubair Port, Iraq

Ayman A. Hassan[1], Husham T. Ibrahim[1*], Ali H. Al-Aboodi[1]

[1] Department of Civil Engineering, College of Engineering, University of Basrah, Basrah, Iraq

* Corresponding author's e-mail: husham.yaseen@uobasrah.edu.iq

**ABSTRACT**

The port of Khour Al-Zubair is located 60.0 km south of the city centre of Basrah; it is also located 105.0 kilometres from the northern tip of the Arabian Gulf. The main goal of this paper is to estimate the concentration of suspended deposit (SSC) in "Khour Al-Zubair" port using a Multilayer Perceptron Neural Network (MLP) based on hydraulic and local boundary parameters while also studying the effect of these parameters on estimating the SSC. Five input parameters (channel width, water depth, discharge, cross-section area, and flow velocity) are used for estimating SSC. Different input hydraulic and local boundary parameter combinations in the three sections (port center, port south, and port north) were used for creating nine models. The use of both hydraulic and local boundary parameters for SSC estimation is very important in the port area for estimating sediment loads without the need for field measurements, which require effort and time.

**Keywords:** suspended sediment concentration, multilayer perceptron, neural network, Khour Al-Zubair port, Basrah city.

## INTRODUCTION

The study and analysis of sediment transport at ports and coastal areas is an important issue in harbor engineering and marine structures; these studies focus on finding solutions to environmental problems such as erosion and deposition in navigational channels or near ocean shores. In particular, there are many problems with coastal structures such as piles, piers, and breakwaters that are of practical and economic importance, especially in the field of harbor engineering and marine structures. Excessive erosion near offshore facilities can affect the stability and durability of "hydraulic structures" like ports and breakwaters, potentially leading to their collapse (M. A. Afshar 2010, K. Babaeyan et al., 2002; H. Bihs, and N. Olsen 2011); on the other hand, increased sedimentation near port berths affects ship draft.

Sediment transport is critical to understanding how sediments are transported and deposited back at other sites. Erosion involves removing and transporting sediments (primarily from a boundary) and then depositing them at other boundaries. Erosion and sedimentation in marine channels and near coastal structures is a very complex matter, as in addition to the well-known influences on rivers, such as the critical velocity of flow and the state of the river bed and its boundaries, there are other influences in coastal areas that have a great impact on the erosion of deposition, namely tides, currents, and waves.

Wave activity is the primary factor in transporting coastal sediments, especially in shallow areas (see wind waves), followed by tides and shore currents. The waves generated by the wind play a major role in transferring energy from the open ocean to the coasts. Usually, during events of large waves, sediment is carted off the seaside look and docks offshore to form a shallow. Since the effective ripple occurrence disappears, the deposits gradually return to shore (Dean et al., 2002). Similarly, the biological procedures that alter the morphology of the coastlines, and the sediment size distribution is other critical factors for changing the state of those coastlines. Human influences and industrial works, in addition to the interactions between physical processes and

coastal landforms, play a role in the modification of these landforms.

In order to assist decision-makers and management, a type of model has been designed for forecasting the amounts of residue transported and the amount of change occurring in the coastal areas, in addition to giving a clear picture of the areas of sedimentation or erosion.

The water of the study area (the estuary of Khour Al Zubair) can be described as a lake environment called a negative estuary, and salinity reaches high levels in the summer months (Al-Ramadhan B.M. 1984). In 1983, an unnatural canal (Shatt Al-Basrah Canal) was established. MOD (the main downstream drain) was related to this channel at 10 kilometres from the top of the canal in 1993; this connection caused an increased in the flow rates which ranged from 100 to 200 $m^3$/sec. Stormwater was drained from Nasiriyah city to the main downstream drain with a discharge of 60 $m^3$/sec. The environment in Shatt Al-Basrah and that of the MOD has become highly saline, with salinity reaching a high level, especially in the summer months.

At the lower strategy of the Khor Al-Zubair waterway, the massive wave forms a perfect geometrical crest. For both floods as well as ebb, the seawater profile was nearly vertical position uniform, with a slight class division continuing to increase toward the lagoon's head (Mahdi A. 1990). Multiple research studies have concentrated on the region under investigation, but a new two-dimensional statistical model is built with the Mike 21 numerical modelling system to investigate how a possible rise in the sea level might affect the hydrodynamic characteristics of the region (Lafta A. 2019). The port of "Khor Al-Zubair" is located on the "Shatt Al-Basrah Canal" and has economic importance, so formula was derived to calculate the sediment transport rate, which was based on local boundaries and hydraulic conditions using the dimensional analysis technique. The total suspended sediment discharge is equal to 1288285.464 tons/year using the proposed formula, while using modelling (1220500.64) tons/year (Dakheel A. 2022).

Artificial neural network applications have gained wide popularity for predicting sediment transport load and other subjects due to their massive functional properties and their long-term predictability, which possess enormous advantages over traditional analysis methods (Van Maanen et al., 2010; Heng 2013; Ebtehaj I. 2013; Duncan W. 2013; Ebtehaj I. et al., 2021).

The main goal of this analysis is to indicate the balanced deposition centration in "Khour Al-Zubair port" operating a multilayer perceptron neural network (MLP) based on hydraulic and local boundary parameters and to investigate the effect of these parameters on predicting suspended sediment load concentration.

## STUDY AREA AND DATA FIELD MEASUREMENTS

The "port of Khour Al-Zubair" is located 60 kilometres south of the city centre of Basrah, and it is also located 105 kilometres from the northern tip of the "Arabian Gulf". This port lies within the "coordinates Margin" ("30° 11' 36'' N") and Longitude ("47° 52' 58" E"). There was a marine canal in Khour Al Zubair that aimed to connect the "Khour Al Zubair Canal" with the Khour Abdullah Canal that leads to the Gulf (Fig. 1). The port has two specialized types of reinforced concrete wharves and iron tubular piles intended for the steel plant. There are two similar adjacent wharves with two 15-ton cranes intended for the import of iron ore, and there are also five specialized wharves at each.

"Khour Al-Zubair port" is discovered within the "Khour AL-Zubair" estuary; a bay consists of a contained portion of moisture linked to the empty sea. The estuarine system includes a flat or water basin and marginal areas around the edge that have been inundated by tidal and storm events. Many different factors interact to shape the estuary's unique characteristics (Shaw and Andrew 2005). The lower boundary can be found close to Umm Qasr port, and the upper boundary can be found close to Khour al-Zubair port. This estuary is 40 kilometres long and is divided into a number of smaller channels that take on a distinctive shape, much like the branches of a tree (see Figure 1). After a flood, the Khour Al-Zubair canal can expand to a width of between one and two kilometres. Ten to twenty meters of water depth is typical. During the ebb and flow of the tides, which occur roughly every 12 hours, there are strong currents and the average tide height is about 3.2 meters (Al-Ramadhan 1988).

It had several days or weeks to select the evaluation channels required for the study and gain the necessary safety authorizations to perform

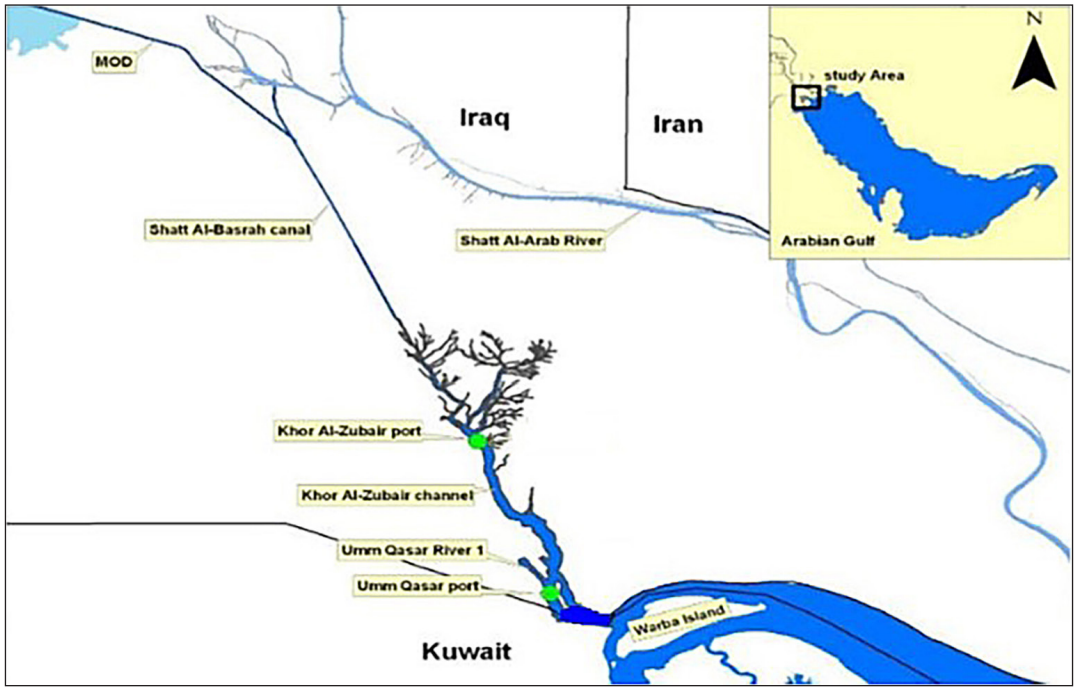


**Figure 1.** Dock of the study area (Lafta et al., 2015)

measurement techniques, so researchers did not start making the trip to the survey area until September 8, 2020 (Dakheel A. 2022). Six transect sections are studied in the field; three are chosen in the immediate future (Oct. 23, 2020–Oct. 25, 2020) and are located at the same sites as those studied for hydraulic properties in the spring (Nov. 30, 2020–Dec. 4, 2020). There are three distinct parts to this area: the first is in front of the Khour Al-Zubair port at (30° 11' 27.84" N, 47° 53' 30.45" E), although the other difference is to the north and south of the dock at (30° 13' 5.73" N, 47° 51' 54.78" E, and (30° 10' 31.48" N, 47° 53' 51.73" E), respectively.

ADCP (Acoustic Doppler Current Profiler) technology is applied for measuring the hydraulic properties of a canal section relating to flow velocity, discharge, cross-sectional area, highest width, and moisture level over double periods (neap and spring) with an hourly log over a full tide cycle (Dakheel A. et al. 2022). "ADCP" is carried on a movable ship along a cross-section of the canal using "WinRiver II software", "ADCP" can calculate real-time discharge while travelling the streamlet and continuously measuring moisture velocity, boat speed, and water depth. Table 1 shows the average measurements of hydraulic properties in the neap and spring periods. The negative sign means that the discharge during the flood period is greater than during the ebb period based on the fieldwork measurements, so it has the opposite direction.

The concentration of suspended sediment usually changes during each tidal period. The concentrations in marine and river environments are much lower than those in estuaries (Doeke, 1993). For measuring the suspended sediment concentrations in the transect sections for the neap and spring periods, vertical sampling was selected at 0.25, 0.5, and 0.75 of the width of

**Table 1.** Hydraulic properties of complete tidal cycle (Dakheel A. 2022)

| Section | Period | Average top width (m) | Average velocity (m/sec) | Average total area ($m^2$) | Average total discharge ($m^3$/sec) |
|---|---|---|---|---|---|
| Port center | Neap | 869.56 | 0.532 | 7051.45 | -98.245 |
| Port South | Neap | 947.73 | 0.595 | 6855.03 | 575.928 |
| Port North | Neap | 558.74 | 0.427 | 2461.45 | 136.141 |
| Port center | Spring | 915.08 | 0.475 | 7477.87 | 386.244 |
| Port South | Spring | 980.99 | 0.554 | 7125.43 | -820.615 |
| Port North | Spring | 614.37 | 0.435 | 2483.96 | -280.801 |

streamflow at each transect. At each vertical station, 3 samples were taken every 2 hours along the tidal period at bottom of 0.2 d, 0.6 d, and 0.8 d, where stands the measured deep from the moisture surface, as illustrated in Figure 2. Table 2 illustrates the average measurements of suspended sediment concentration (SSC) in the neap and spring periods.

According to Dakheel A. 2022, the sample is lifted from each station by using a point-integrating sampler, which was designed to collect the samples at specific points. The discontinued load attention is defined in the laboratory. The cross-section 9 samples at 2 hours were wrapped in a black-coloured cover until it reaches the laboratory in order to preserve the sample's quality. It uses a glass filtration system with a vacuum to filter samples. The concentration of broken sediment is estimated utilising the following equation (Dakheel and Al-Aboodi. 2022):

$$ssc = \frac{m}{v} \tag{1}$$

where: $ssc$ – concentration of suspended sediment load (kg/m$^3$, mg/l, or PPM);
$m$ – mass of the sediment load (mg);
$v$ – water volume (L).

**Table 2.** Suspended sediment concentration (SSC) of complete tidal cycle

| Section name | Period | SSC (mg/l) |
|---|---|---|
| Port center | Neap | 307.04 |
| Port South | Neap | 290.17 |
| Port North | Neap | 130.49 |
| Port center | Spring | 81.47 |
| Port South | Spring | 150.89 |
| Port North | Spring | 122.68 |

## MULTILAYER PERCEPTRON NEURAL NETWORK

A "multilayer perceptron (MLP)" is a totally related variety of "artificial neural networks" (ANN). The term "MLP" stands for ambiguity or is loosely expressed to suggest any forward-oriented ANN, occasionally to refer precisely to webs made up of numerous layers of perception. MLP consists of three layers of nodes, as illustrated in Figure 3; the layers are sequenced from left to right as an input layer, a hidden layer, and an output layer. These nodes are neurons that use a "non-linear activation function" except for the input nodes. The backpropagation algorithm is used as a supervised learning method for training in MLP.

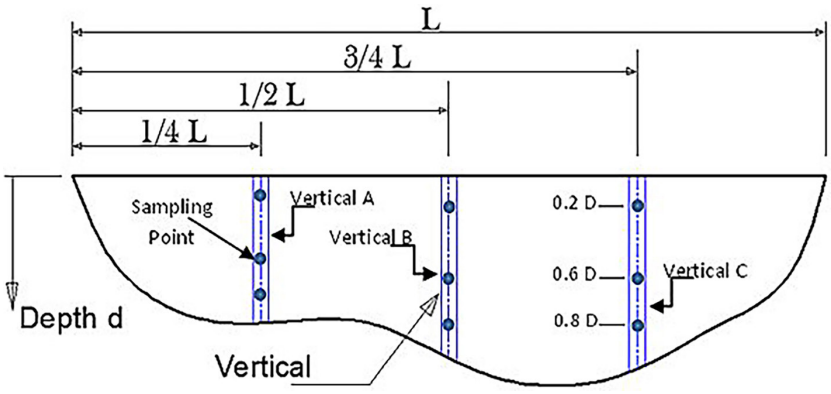


**Figure 2.** Suspended sediment sampling columns (Dakheel A. 2022)

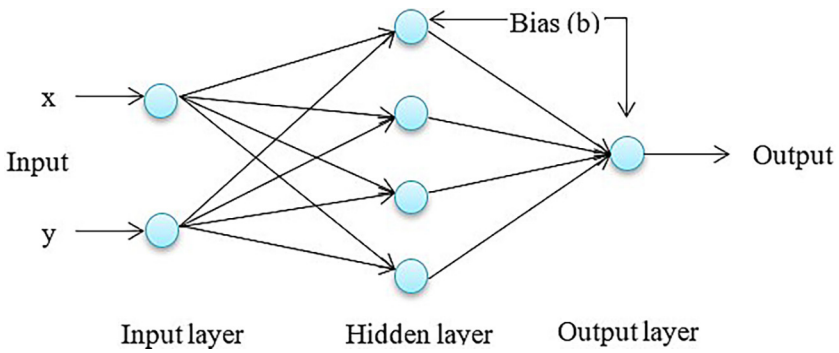


**Figure 3.** Architecture of an MLP with one secret layer

A scalar weight ($w$) is used for weighting the connection between processing elements (PEs). During the process of training, the scalar weight is adopted. Through the training process, the connection importance is modified to decrease the squared contrast between the expected result and the PE reply. The "optimal weights" ($w_{opt}$) are produced from the cross-correlation vector (P) and the inverse input autocorrelation matrix ($R^{-1}$). It can be said that the "analytical solution" in this method is identical to the examination process used to discover the lowest cover "quadratic performance", J ($w_i$), operating angle descent by changing the importance at per epoch (Ivakhnenko 1971).

$$w_i(k+1) = w_i(k) - \eta \nabla J_i(k)$$
$$\nabla J_i = \frac{\partial J}{\partial w_i} \quad (2)$$

where: $\eta$ – coefficient of understanding velocity;
$\nabla J_i(k)$ – gradient vector of the implementation cover for the ith information node at iteration $k$.

Equation 3 is utilised for obtaining the implementation surface (J):

$$J = \sum_{P} \left(d_p - y_p\right)^2 \; and$$
$$J \rightarrow w_{opt} = R^{-1}P \quad (3)$$

where: $d_p$ – target vector;
$y_p$ – output of the p$^{th}$ output neuron.

## METHODOLOGY

A multilayer perceptron neural network is applied for predicting the "suspended sediment concentration" in "Khour Al-Zubair port". Five input hydraulic and local boundary parameters (channel width, water depth, discharge, cross-section area, and flow velocity) are used for predicting the SSC. Different input hydraulic and local boundary parameter combinations in the three sections (port centre, port south, and port north) were used for creating nine models. A different set of inputs was used to study their effect on the models' outputs. The use of both hydraulic and local boundary parameters to estimate the SSC is very important in the port area in order to infer these quantities without the need for field measurements, which require effort and a long time. Also, through the outputs of the models, the most important parameters will be revealed, as well as the need for studies of new parameters. The combinations of input parameters and the applied model numbers are illustrated in Table 3. The network will be built using 20 neurons for hidden layer; network size evaluation was performed using 5-fold cross-validation.

The variables that are sent in can be split up into two distinct groups (training and testing). During the training phase of development, the framework of artificially intelligent model systems is put into place. "Testing data" that was not operated in the training process is applied to trained standards in order to evaluate the precision of the model's predictions. Certain proportions of events are applied during the training and testing process. Because of this, when different proportions of input data are used, different results and conclusions are presented (Ming and Gwo 2015). In order to find a solution to this issue, the authors of this paper made use of cross-validation. In this process, the performance of an artificial neural model is evaluated via cross-validation. This is done by selecting a group of rows for a per fold that is then randomly checked on the target variable "SSC." The network size was determined through the use of a 5-fold cross-validation procedure.

All models use a maximum of three layers of the MLP algorithm (an input layer; one hidden layer and an "output layer"). The range of weights is standardized with the help of the input

**Table 3.** Multilayer perceptron neural network models with input parameters combinations

| Model No. | Section name | Input parameters | Model No. | Section name | Input parameters |
|---|---|---|---|---|---|
| 1 | Port center | All parameters | 6 | Port North | Discharge, cross section area, and flow velocity |
| 2 | Port South | All parameters | 7 | Port center | Flow velocity |
| 3 | Port North | All parameters | 8 | Port South | Flow velocity |
| 4 | Port center | Discharge, cross section area, and flow velocity | 9 | Port North | Flow velocity |
| 5 | Port South | Discharge, cross section area, and flow velocity | | | |

**Table 4.** Optimum number of neurons in hidden layer of Model 2

| No. of neurons | Residual variance % | No. of neurons | Residual variance % |
|---|---|---|---|
| 2 | 82.52848 | 8 | 82.35286 |
| 3 | 86.92666 | 9 | 91.84951 |
| 4 | 87.99339 | 10 | 84.52846 |
| 5 | 87.24114 | 11 | 84.35436 |
| 6 | 85.34697 | 12 (Optimal size) | 80.44416 |
| 7 | 86.34201 | 13 | 88.25472 |

**Table 5.** Convergence Parameters of All Models

| No. convergence tries | 4.00 | Iterations without improvement | 100.00 |
|---|---|---|---|
| Maximum iterations | 10000 | "Convergence tolerance" | 1.000e-0050 |
| Minimum improvement delta | 1.000e-0060 | Minimum gradient | 1.000e-0060 |

neurons, and the oracle variable can take on matters ranging from -1 to 1. The hidden layer neurons receive the predictor variables, which are then used to train the model. The weight is then multiplied by the bias constant before it is fed to the output layer (Fig. 3). By specifying a maximum and a minimum value for a lot of neurons in the hidden layer, it is possible to obtain an optimal lot of neurons in the layer automatically. Through the use of Model 2, one can get an idea of what the ideal number of neurons is by observing the data in Table 4. This procedure is carried out by first generating a large number of models, each of which has a different total lot of neurons in the invisible layer, and then using a cross-validation training procedure to evaluate how well each model performed.

The scaled conjugate gradient algorithm is used in the process of updating the values of weight; this method is carried out by errors propagating backwards through the network. Logistic and linear activation functions, respectively, are the types that are utilized by the hidden and output activation processes. The effectiveness of MLP models during the training and testing phases is assessed using RMSE ("Root Mean Squared Error"), MSE ("Mean Squared Error"), MAE ("Mean Absolute Error"), and MAPE ("Mean Absolute Percent Error") ("Mean Absolute Percentage Error"). Table 5 contains a presentation of all the models' additional convergence parameters.

## RESULTS AND DISCUSSION

The optimum solution number of neurons required for each hidden neuron is based on the remaining variables (per cent). As illustrated in Table 6, an increase in the number of predictors does not necessarily indicate a rise in the number of neurons. Table 6 illustrates the optimal size of neurons for all models. In general, it is noted that the minimum optimal number of neurons is not less than 4 in these models. Also, the decrease in the residual variance % is not observed with the increase in the number of predictors. This can be attributed to the complexity of the problem and the fact that some predictors do not affect the efficiency of the model. There is another effect on the efficiency of the models, as some parameters were entered as of one value for one section with different values of sediment concentration, for example, the top width of the water section, total discharge, and total section area.

As shown in Table 7, the implementation of the MLP standard in both activity and validation steps are estimated based on RMSE, MSE, MAE, and MAPE. It is noticed from this table that the values of the statistical parameters vary between the models and that each section has

**Table 6.** Neurons optimal size of MLP models using 5-fold cross-validation

| Model No. | Optimal size of neurons | Residual variance % |
|---|---|---|
| 1 | 20 | 46.53653 |
| 2 | 12 | 80.44416 |
| 3 | 7 | 81.01759 |
| 4 | 5 | 47.43312 |
| 5 | 20 | 82.61717 |
| 6 | 4 | 88.60143 |
| 7 | 8 | 72.11570 |
| 8 | 3 | 95.37982 |
| 9 | 4 | 92.25550 |

characteristics that distinguish it from the rest of the sections. It is noted, for example, that in the port centre section, which includes the models (one, four and seven) (see Table 3), as it is shown by raising the number of predictors, the efficiency of the model increases and the difference between the calculated and target value decreases, this rule applies to all models except for a few exceptions. Through the statistical parameter (MAPE), the efficiency of the first model exceeded the efficiency of the fourth and seventh models by a percentage of 12.3% and 46.2%, respectively. It can be said that increasing the number of predictors for the study area models increases the efficiency of the model in estimating the sediment concentration.

It is also possible to take advantage of the correlation coefficient (R) to get an idea of the success or failure of these models in estimating the quantities of sediments in the study area. Table 8 shows the correlation coefficients for the verification phase.

**Table 7.** MLP model performance according to statistical criteria

| Model No. | | RMSE | MSE | MAE | MAPE |
|---|---|---|---|---|---|
| 1 | Training | 139.29477 | 19403.034 | 78.708577 | 87.550493 |
| | Validation | 170.95821 | 29226.709 | 106.40193 | 130.05348 |
| 2 | Training | 203.8026 | 41535.498 | 129.40182 | 146.63426 |
| | Validation | 218.52088 | 47751.373 | 142.33581 | 153.48398 |
| 3 | Training | 91.665479 | 8402.5601 | 61.555574 | 97.952268 |
| | Validation | 100.31801 | 10063.704 | 69.654617 | 105.36607 |
| 4 | Training | 160.39948 | 25727.993 | 99.346362 | 123.97206 |
| | Validation | 175.47223 | 30790.504 | 112.04109 | 146.5501 |
| 5 | Training | 209.46557 | 43875.824 | 137.71994 | 153.02719 |
| | Validation | 220.64682 | 48685.02 | 147.05861 | 160.43119 |
| 6 | Training | 96.810355 | 9372.2448 | 70.124647 | 110.73461 |
| | Validation | 99.136378 | 9828.0215 | 70.987657 | 113.61726 |
| 7 | Training | 191.52843 | 36683.14 | 130.93314 | 184.9363 |
| | Validation | 202.41114 | 40970.269 | 137.44898 | 190.6708 |
| 8 | Training | 236.49263 | 55928.766 | 167.9922 | 211.44588 |
| | Validation | 237.79384 | 56545.909 | 165.53158 | 202.07378 |
| 9 | Training | 97.496468 | 9505.5613 | 72.568871 | 126.86463 |
| | Validation | 99.529394 | 9906.1004 | 73.519496 | 123.96396 |

**Table 8.** The correlation coefficients for validation phase

| Model no. | *R* | Model No. | *R* | Model no. | *R* |
|---|---|---|---|---|---|
| 1 | 0.882 | 4 | 0.656 | 7 | 0.497 |
| 2 | 0.762 | 5 | 0.623 | 8 | 0.278 |
| 3 | 0.680 | 6 | 0.575 | 9 | 0.266 |

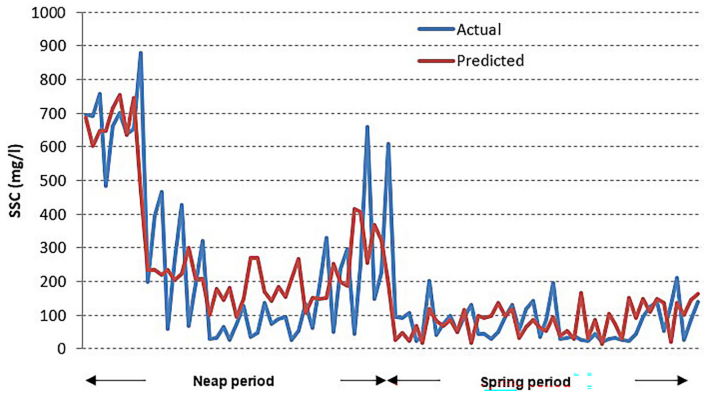


**Figure 4.** Comparative plot of measuring SSC versus estimating SSC by model no. 1

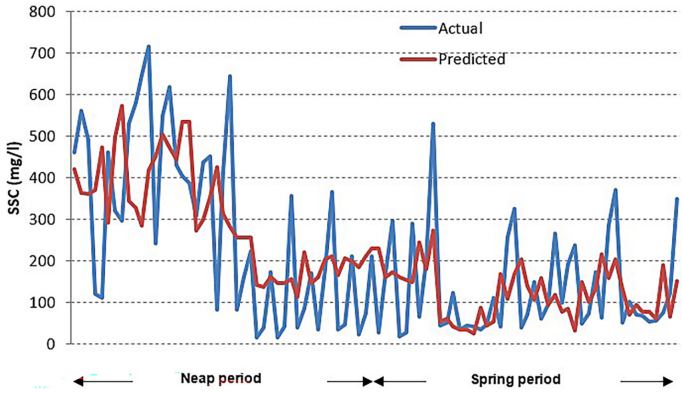


**Figure 5.** Comparative plot of measuring SSC versus estimating SSC by model no. 2

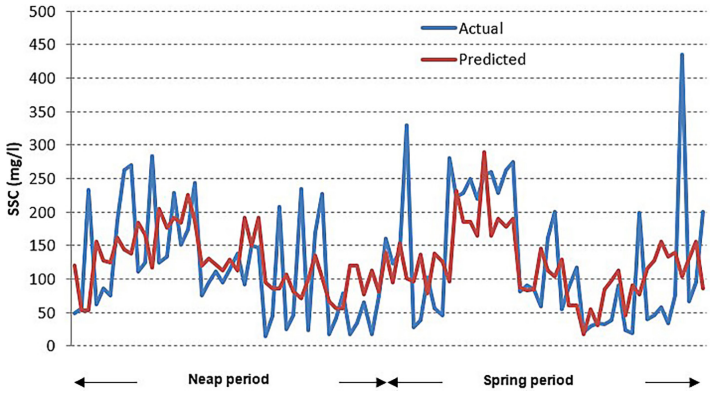


**Figure 6.** Comparative plot of measuring SSC versus estimating SSC by model no. 3

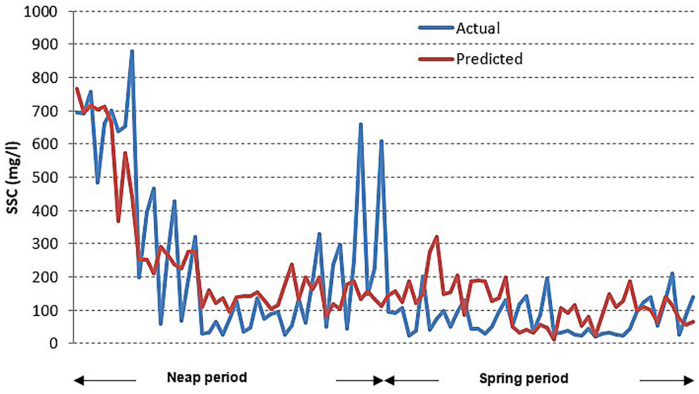


**Figure 7.** Comparative plot of measuring SSC versus estimating SSC by model no. 4

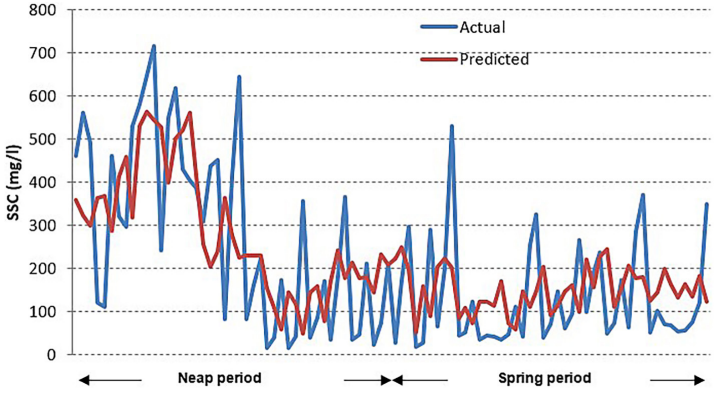


**Figure 8.** Comparative plot of measuring SSC versus estimating SSC by model no. 5

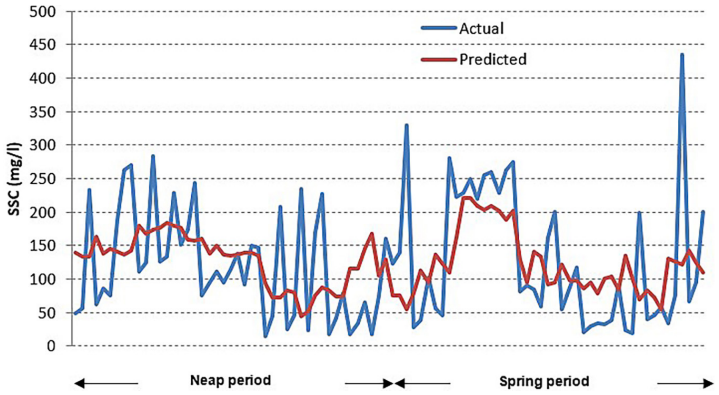


**Figure 9.** Comparative plot of measuring SSC versus estimating SSC by model no. 6

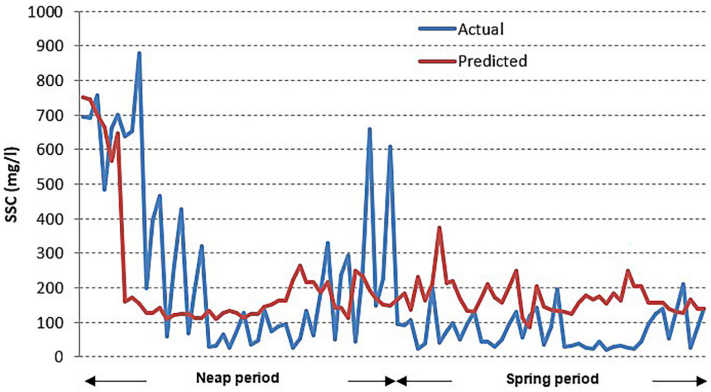


**Figure 10.** Comparative plot of measuring SSC versus estimating SSC by model no. 7

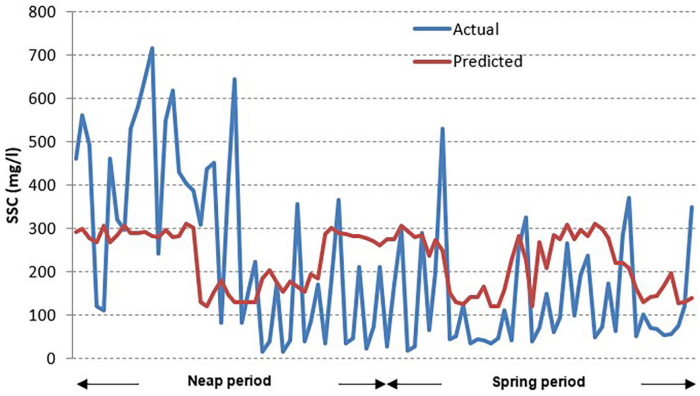


**Figure 11.** Comparative plot of measuring SSC versus estimating SSC by model no. 8

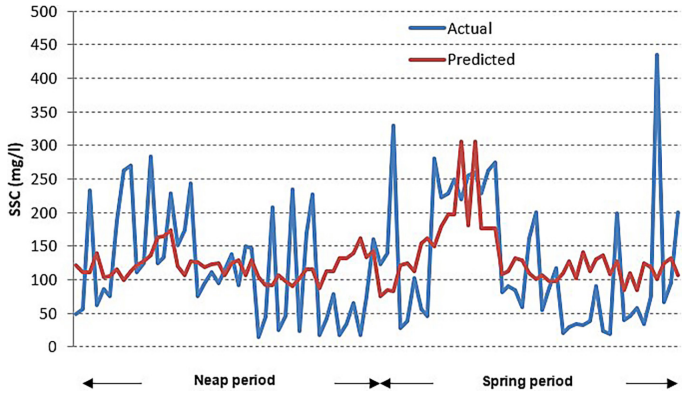


**Figure 12.** Comparative plot of measuring SSC versus estimating SSC by model no. 9

The correlation weight between the calculated and measured "sediment concentration" values of MLP models can be observed from Table 8, where it appears that the models (one, two, and three) have a relatively high correlation value compared to the rest of the models, as it is inferred that increasing the number of predictors aims to improve the efficiency of the model. While the models (four, five, and six) had relatively moderate correlation values due to the decrease in the number of predictors, for the models (seven, eight, and nine), the correlation values were reduced as only the flow velocity was used to estimate the sediment concentration, where it can be concluded that using the value of the flow velocity alone is not preferred in estimating the sediment concentration in the study area.

The efficiency of the models may be enhanced by introducing other variables involved in the estimation process, such as water levels, specific gravity, and grain size analysis of bed materials. The comparative plots of the training and validation phases for measuring SSC values and estimating values by the MLP model are shown in Figs. 4 to 12.

## CONCLUSIONS

A MLP neural network is applied for predicting the SSC in Khour Al-Zubair port. Five inputs, including hydraulic and local boundary parameters (channel width, water depth, discharge, cross section-area, and flow velocity), are used for predicting the SSC. The increasing number of predictors increased the efficiency of the model and decreased the contrast between the calculated weight and the mark weight. It became clear through modelling that the models with five predictors outperformed the rest of the models. The models with three input variables had relatively moderate correlation coefficients, but as for the models with one input variable (flow velocity), the correlation values were reduced, and it can be concluded that using the value of the flow velocity alone is not preferred in estimating the SSC in the study area.

## REFERENCES

1. Al-Ramadhan B.M. 1988. Residual fluxes of water in an estuarine lagoon", Estuarine, Coastal and Shelf Science, 26, 319–330.
2. Al-Ramadhan B.M. 1987. Salinity distribution in Khor Al-Zubir, South of Iraq. Mahasagar-Bulletin of the National Institute of Oceanography, 20, 145–154.
3. van Maanen B., Coco G., Bryan K.R., Ruessink B.G. 2010. The use of artificial neural networks to analyze and predict alongshore sediment transport. Processes Geophys., 17, 395–404.
4. Dakheel A.A. 2022. Sediment Transport Modelling in Khour Al-Zubair Port, South of Iraq " PhD thesis, University of Basrah, College of Engineerin.
5. Dakheel A.A., Al-Aboodi A.H., Abbas S.A. 2022. An empirical formula development to predict suspended sediment load for Khour Al-Zubair port, South of Iraq, Open Engineering, 12, 169–175.
6. Dakheel A.A., Al-Aboodi A.H., Abbas S.A. 2022. Investigation for hydrodynamic processes of water in Khour Al-Zubair Port using hydrodynamic model, Materials Today: Proceedings, 61(3), 1073–1082.
7. Dean, R.G., Dalrymple R.A. 2002. Coastal Processes: With Engineering Applications. Cambridge, UK New York: Cambridge University Press.
8. Doeke E. 1993. Suspended Matter in the Aquatic Environment. Springer Verlag, 1st edition.
9. Duncan W. 2013. Thermal energy from a biogas plant for leachate treatment. Energies, 15(3), 753–767.
10. Ebtehaj I., Bonakdari H. 2013. Evaluation of Sediment Transport in Sewer Using Artificial Neural Network. Eng Appl Comput Fluid Mech, 7(3), 382–392.
11. Ebtehaj I., Bonakdari H., Zaji A.H., Gharabaghi B. 2021. Evolutionary optimization of neural network to predict sediment transport without sedimentation. Complex and Intelligent Systems, 7, 401–416.
12. Bihs H., Olsen N. 2011. Numerical modeling of abutment scour with the focus on the incipient motion on sloping beds. Journal of Hydraulic Engineering, 137(10), 1287–1292.
13. Chanson H. 2004. The hydraulics of open channel flow: An introduction. Elsevier Butterworth-Heinemann.
14. Heng S., Suetsugi T. 2013. Using Artificial Neural Network to Estimate Sediment Load in Ungauged Catchments of the Tonle Sap River Basin, Cambodia. Journal of Water Resources abd Protection, 5(2).
15. Ivakhnenko A.G. 1917. Polynomial theory of complex systems", IEEE Trans., Syst. Man Cybern. MC-1. 4, 364–378.
16. Babaeyan-Koopaei K., Ervine D., Carling P., Cao Z. 2020. Velocity and turbulence measurements for two overbank flow events in river severn. Journal of Hydraulic Engineering, 128(10), 891–900.
17. Lafta A.A. 2019. Numerical Modeling for Field Study of physical Characteristics in Iraqi Marine Water, PhD thesis, University of Basrah, College of Education of pure science.

18. Lafta A.A., Al-Taei S.A., Al-Fartusi A.J. 2015. One dimensional hydrodynamics model for Khour Al-Zubair channel, South West of Iraq. J Int Academic Res Multidiscip, 3(4), 437–445.
19. Afshar M.A. 2010. Numerical wave generation in Open FOAM. Master's thesis, Chalmers University of Technology, 2010.
20. Mahdi A.A.J. 1990. Mixing and Circulation of The water Mass in The Khour Al-Zubair", M.Sc. thesis, University of Basrah, The Marine Science Center.
21. Ming-Chang W., Gwo-Fong L. 2015. An Hourly Streamflow Forecasting Model Coupled with an Enforced Learning Strategy. Water, 7, 5876–5895.
22. Shaw M., Moores A. 2005. Estuary Sedimentation: a Review of Estuarine Sedimentation in the Waikato Region", Marine Consulting and Research, Environment Waikato Technical Report Series.